J. Membrane Biol. 69, 199–212 (1982)

The Journal of
Membrane Biology

Morphology of the Intermediate Stages in the Lamellar to Hexagonal Lipid Phase Transition

Valery L. Borovjagin*, Juan A. Vergara**, and Thomas J. McIntosh**

* Institute of Biological Physics, Academy of Science of the USSR, Puschino, Moscow Region, 142292 USSR, and
** Department of Anatomy, Duke University Medical Center, Durham, North Carolina 27710

Summary. The addition of calcium to suspensions of egg phosphatidylcholine and cardiolipin converts multiwalled liposomes to the hexagonal (H_{II}) phase (Rand, R.P., Sengupta, S. (1972) *Biochim. Biophys. Acta* **255**:484–492). We have studied this lamellar to hexagonal phase transition by freeze-fracture, thin-section electron microscopy, and X-ray diffraction and have morphologically characterized the intermediate stages. The first step in the transition involves the invagination and fusion of bilayers, marked by the appearance of lipidic intramembrane particles and "crater-like" indentations, as the large liposomes are converted to smaller flattened and elongated vesicles. The next step is the formation of tightly packed hexagonal arrays of tubules, each tubule being about 11 to 15 nm in diameter. These tubules are filled with fluid and a lipid bilayer forms the wall of each cylinder. Finally this tubular bilayer phase is converted to the hexagonal (H_{II}) phase, where the distance between tubes is 5.5 to 7.5 nm.

Key Words cardiolipin · hexagonal phase · lamellar phase · lipid polymorphism · phase transition · freeze fracture

Introduction

Hexagonal lipid phases are of interest for a number of reasons. First, several isolated membrane lipids organize in hexagonal phases under physiological conditions (Gulik-Krzywicki, Rivas & Luzzati, 1967; Junger & Reinauer, 1969; DeGrip et al., 1979; Burnell, Van Alphen, Verkleij & DeKruijff, 1981; Cullis et al., 1980). Many membrane lipids and other lipids are polymorphic and convert from the bilayer (lamellar) phase to the hexagonal phase as a function of hydration, temperature, or divalent cation concentration (Luzzati & Husson, 1962; Tardieu, Luzzati & Reman, 1973; Rand & Sengupta, 1972). The fusogen oleic acid produces hexagonal phases in red blood cell ghost membranes (Cullis & Hope, 1978). Moreover, hexagonal phases have recently been found in inclusions *in vivo* in retinal rod outer segments (Corless & Costello, 1981) and in experimental lipidosis in retinal pigment epithelium (Buchheim, Drenckhahn & Lullmann-Rauch, 1979).

There have been several recent studies on the bilayer to hexagonal transition in the case of membrane lipid (Verkleij et al., 1979, 1980; Van Ventie & Verkleij, 1981; Hui, Stewart, Yeagle & Albert, 1981). Of particular interest in these studies have been the intermediate phases in the transition, which may have biological significance (Cullis & DeKruijff, 1979; Hui et al., 1981). One intermediate stage that has been described is a bilayer phase containing particles and pits. The nature of these "lipidic particles" and their role in the bilayer to hexagonal transition is controversial (Miller, 1980; Verkleij et al., 1980; Borovjagin & Vasilenko, 1981; Hui, Stewart, Boni & Yeagle, 1981; Rand, Reese & Miller, 1981). A recent model proposes that the lipidic particles are inverted micelles and that large inverted micelles provide an intermediate stage in the bilayer to hexagonal transition (Van Venetie & Verkleij, 1981).

The purpose of this present paper is to characterize morphologically the intermediate stages or phases in the bilayer-hexagonal transition. We have examined this transition in defined mixtures of phosphatidylcholine (PC) and cardiolipin (CL). Cardiolipin is a major phospholipid of the inner mitochondrial membrane and has been shown to form the hexagonal (H_{II}) phase in the presence of equimolar calcium (Rand & Sengupta, 1972). The hexagonal (H_{II}) phase consists of long rods of indefinite length, packed in an hexagonal array (Luzzati & Husson, 1962). The center of each rod contains a fluid channel, with the lipid molecules arranged so that the polar heads surround the channel and the hydrocarbon tails extend radially from the cylinder axis.

Materials and Methods

Cardiolipin and egg yolk lecithin were obtained from Sigma Chemical Company (St. Louis) and Lipid Products (Nutfield,

0022-2631/82/0069-0199 $02.80

England), respectively. Lipid suspensions were made by the following procedures. Appropriate mixtures of egg PC and cardiolipin (3:1, 1:1, 1:3, and 1:5 molar ratios) were removed from ethanol solutions by rotary evaporation. Excess (70% by weight) water was added to the dry lipid. The suspension was extensively vortexed and allowed to equilibrate for several hours. It is known that the hexagonal phase precipitates from appropriate PC/CL mixtures upon the addition of calcium (Rand & Sengupta, 1972). Since for most experiments we were interested in studying intermediate stages in hexagonal phase formation, small amounts of 20 mM $CaCl_2$ were added to the lipid phase and vortexed until precipitates could first be observed, either by eye or by light microscopy. Samples for electron microscopy and X-ray diffraction analysis were taken at various times (from 1 to 26 hr) after the $CaCl_2$ was added, depending on whether early or late stages in hexagonal phase formation were to be analyzed. To be certain of the appearance of the final equilibrium hexagonal phase, in one series of experiments we added excess 20 mM $CaCl_2$ to dried cardiolipin and allowed the calcium cardiolipin to fully precipitate (shown in Fig. 8).

Freeze Fracture

Freeze-fracture experiments were performed by the techniques described by Costello and Corless (1978). Small samples, about 0.1 μl, prepared without cryoprotectants were placed between two copper strips. These specimens were then plunged into liquid propane (−190 °C) at sample cooling rates in excess of 10,000 °C/sec (Costello, 1980). The frozen samples were inserted into a hinged double replica device adapted for use on a Balzers BA 360 freeze-fracture unit. Fracturing was done at −155 °C and about 10^{-7} torr. Some samples, as indicated in the figure legends, were etched for 15 sec at −99 °C. Samples were replicated with platinum from a 45° angle and carbon from a 90° angle. The replicas were cleaned in Clorox®, washed in water, picked up on uncoated 400-mesh electron microscope grids, and examined with a Philips 300 or 301 electron microscope equipped with an anticontamination device cooled with liquid nitrogen. All freeze-fracture micrographs are mounted so that the platinum deposition direction is approximately from the bottom.

Thin Sectioning

For thin sectioning, the lipid suspensions were deposited on the shiny side of a Millipore filter (Millipore Corp., Radford, Mass.), with pore size 0.025 μm, which was placed on top of three or four layers of Whatman #1 filter paper. A drop of 2.5% glutaraldehyde and 1% tannic acid in Hepes buffer, pH 7.8, was deposited on top of the lipid suspension. The Millipore filter was then pierced with a pointed instrument to allow the fixative to diffuse slowly through the sample. This operation was repeated three times. The Millipore filter was inverted on a drop of fixative and left in a closed plastic Petri dish for an additional 15 min. The sample was washed by immersing the Millipore filter 10 times in Hepes buffer and postfixed with 0.25% osmium tetroxide for 15 min. We note that Kalina and Pease (1977) have shown that model systems containing phosphatidylcholine are well preserved by similar tannic acid/osmium tetroxide fixation procedures. The specimen was then block stained in 1% uranyl acetate in 10 mM sodium acetate, dehydrated in an ethanol series, and embedded in Epon 812. Thin sections were cut on a Reichert OmU2 microtome and examined with a Philips 301 electron microscope. Optical diffraction patterns of selected micrographs were obtained using an optical diffractometer built by Dr. William Longley of the Anatomy Department at Duke University.

X-ray Diffraction

For X-ray diffraction experiments, specimens were sealed in quartz-glass X-ray capillary tubes and mounted in a pinhole camera equipped with a flat plate film cassette. Diffraction patterns were recorded as described previously (McIntosh, Simon & MacDonald, 1980).

Results

Suspensions of PC/CL (1:1 mole ratio) in excess water contain multiwalled liposomes of various sizes (Fig. 1 *A*). The fluid layers between bilayers generally are wide (Fig. 1 *A*, arrow). After the addition of calcium, these samples show many examples of intermembrane contacts and points of fusion (arrowheads in Fig. 1 *B*). After longer incubation with calcium, extensive fusion (Fig. 1 *C*) and formation of small unilamellar vesicles (Fig. 1 *D*) can be seen.

Figure 2 shows a similar phenomenon in a 1:3 PC/CL mixture after the addition of calcium. The thin section in Fig. 2 *A* shows that the disruption of the multiwalled vesicular structure starts from the outside of the vesicle where the calcium has been introduced. The asterisk marks the inside of the liposome. Small vesicles or tubular bilayer structures pinch off from the outside lamellae. Figure 2 B is a higher magnification view of the same process, showing that in each instance the multiwalled vesicle is converted to bilayer structures with much smaller radii of curvature. Occasionally close packed, apparently lamellar, structures are also observed (arrowhead, Fig. 2 *B*). Figure 2 *C* is a freeze-fracture image of the same specimen, showing small unilamellar vesicles as well as large flattened vesicles near the center of the field. A tight packing of several vesicles is seen in Fig. 2 *D* (arrowhead).

Other views in the conversion to the hexagonal phase are shown in Fig. 3. Different degrees of bilayer fusion are seen in Fig. 3 *A–C*. Note the particles, pits, and ridges in the fracture faces (small arrowheads). Parallel rows or striations in the fracture planes can be seen in Fig. 3 *A* (large arrowhead), in 3 *B* (center of field), and in 3 *C* (marked by asterisk). These striations have a periodicity of between 7 and 12 nm. Note that the ridges and furrows in the bilayers can be parallel (Fig. 3 *A* and *B*) or perpendicular (Fig. 3 *C*, small arrowheads) to the striations. Figure 3 *D* shows the spatial relationship among small vesicles (small arrowheads), flattened vesicles (arrow), and the stria-

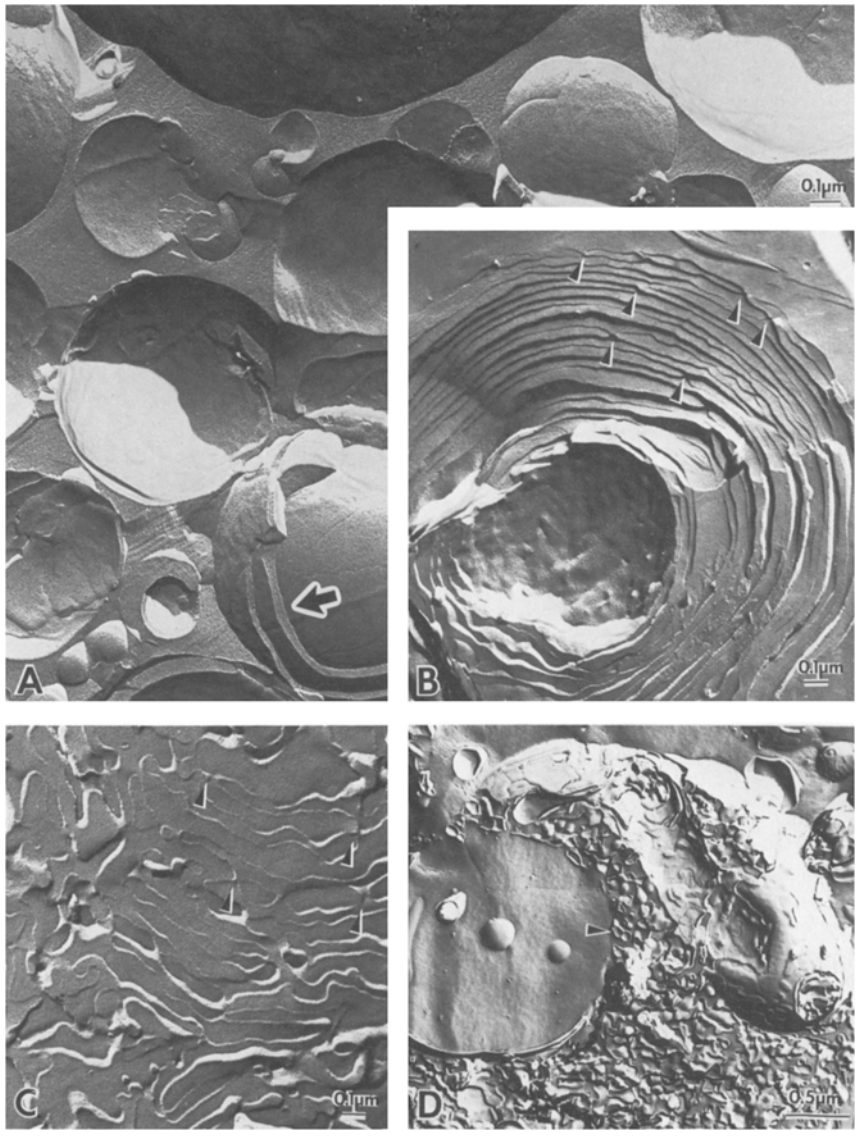

Fig. 1. Freeze-fracture electron micrographs of 1:1 molar mixtures of egg phosphatidylcholine and cardiolipin. Image *A* is the control preparation in pure water while (*B–D* shows the same specimen after the addition of calcium chloride (*see* text for details). In *B*, the specimen was frozen 2 hr after the addition of calcium, while in *C* and *D* the incubation time was 6 hr

tions. A close examination of Fig. 3*D* shows many other examples of direct continuity between small vesicles and the striated regions and between the flattened bilayers and the striations.

Figure 4*A* shows the appearance of the inside of a PC/CL liposome after a long incubation with calcium. Tightly packed small vesicles and striated surfaces (upper right hand corner) can be seen. Often the striations run in different directions, as shown in Fig. 4*B*, where the rows in the center of the field are almost perpendicular to the rows at the right and left edges of the field. There are two distinct periodicities in the striated regions. A separation between rows of approximately 6.7 nm is seen in some areas (small arrowhead), while a larger separation of about 11.0 nm (large arrowhead) is seen in other regions. Occasionally (for example, below the small arrowhead) the large and small periodicity striations can be seen running together. Direct continuity between the striated facture faces and flattened bilayers is seen in the lower left-hand corner of Fig. 4*B*. In Figure 4*C*, two regions of striated fracture faces (marked by asterisks) can be seen surrounded by small and flattened vesicles and crater-like protrusions on the fracture face of a larger bilayer surface. The crater-like images seen in the center of the field (arrowheads) are evidence of the small vesicle formation.

Figure 5 provides more detail about the structure of the striated regions and the surrounding small vesicles. In some areas (large arrowhead in Fig. 5*A* and large and small arrowheads in 5*B*) cross fractures of the striations are present. In these areas it can be seen that striations represent an

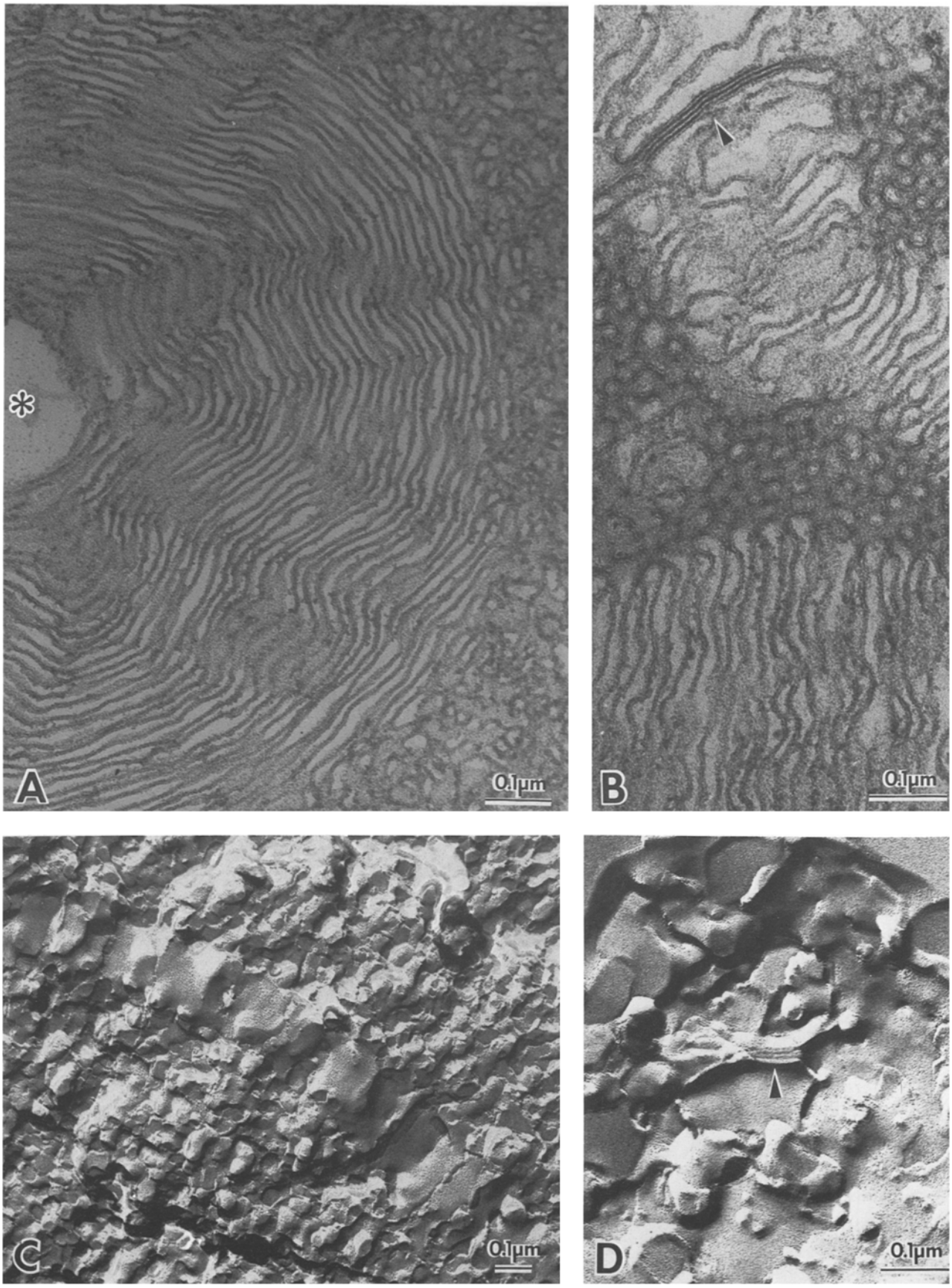

Fig. 2. Thin-section (*A* and *B*) and freeze-fracture (*C* and *D*) images of a 1:3 molar ratio of PC/CL 2 hr (*D*) and 6 hr (*A–C*) after the addition of calcium chloride. In *A* the asterisk marks the center of the multiwalled PC/CL liposome

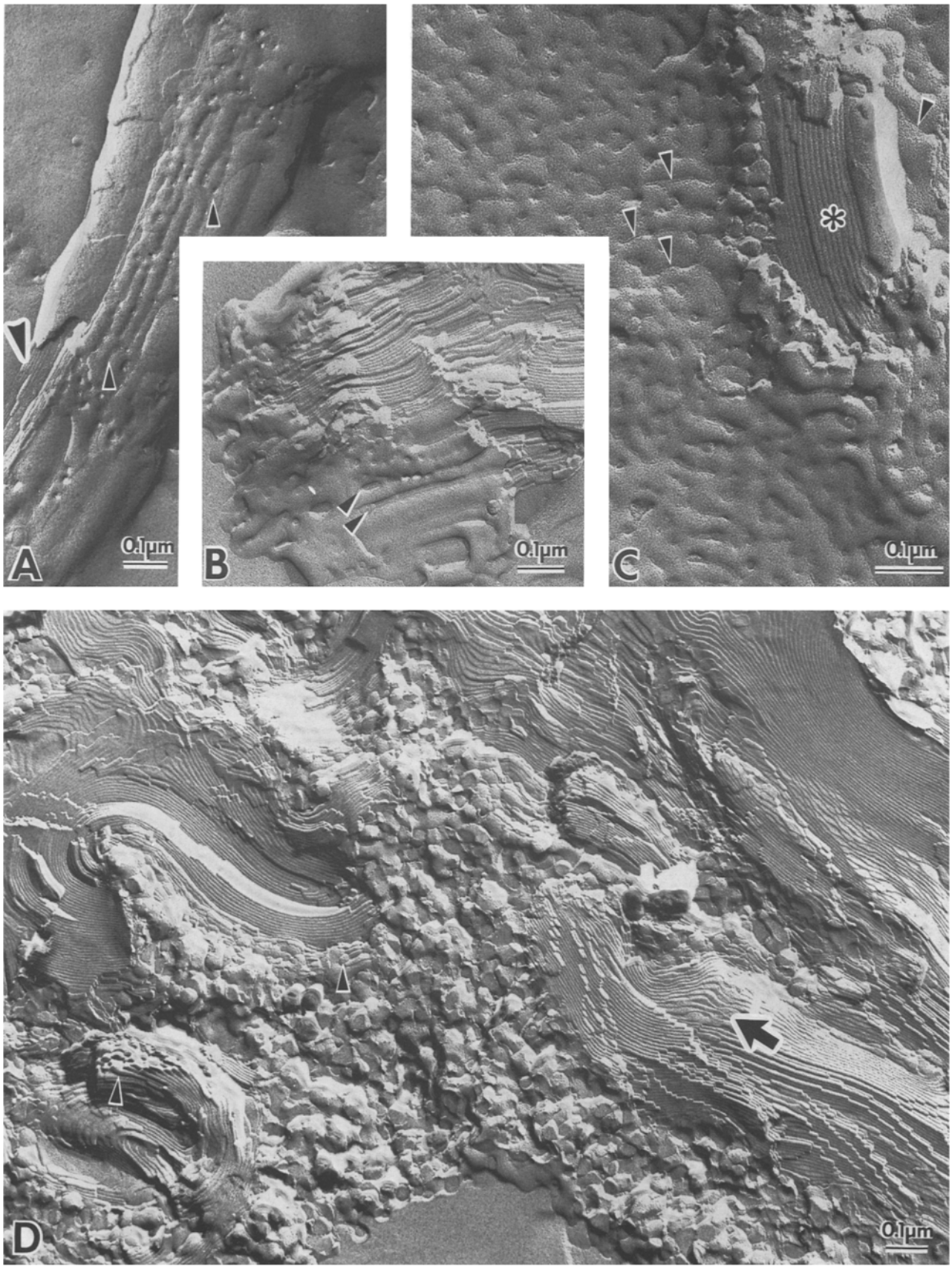

Fig. 3. Freeze-fracture images of a suspension of 1:1 molar ratio PC/CL 6 hr (*A–C*) and 12 hr (*D*) after the addition of calcium chloride

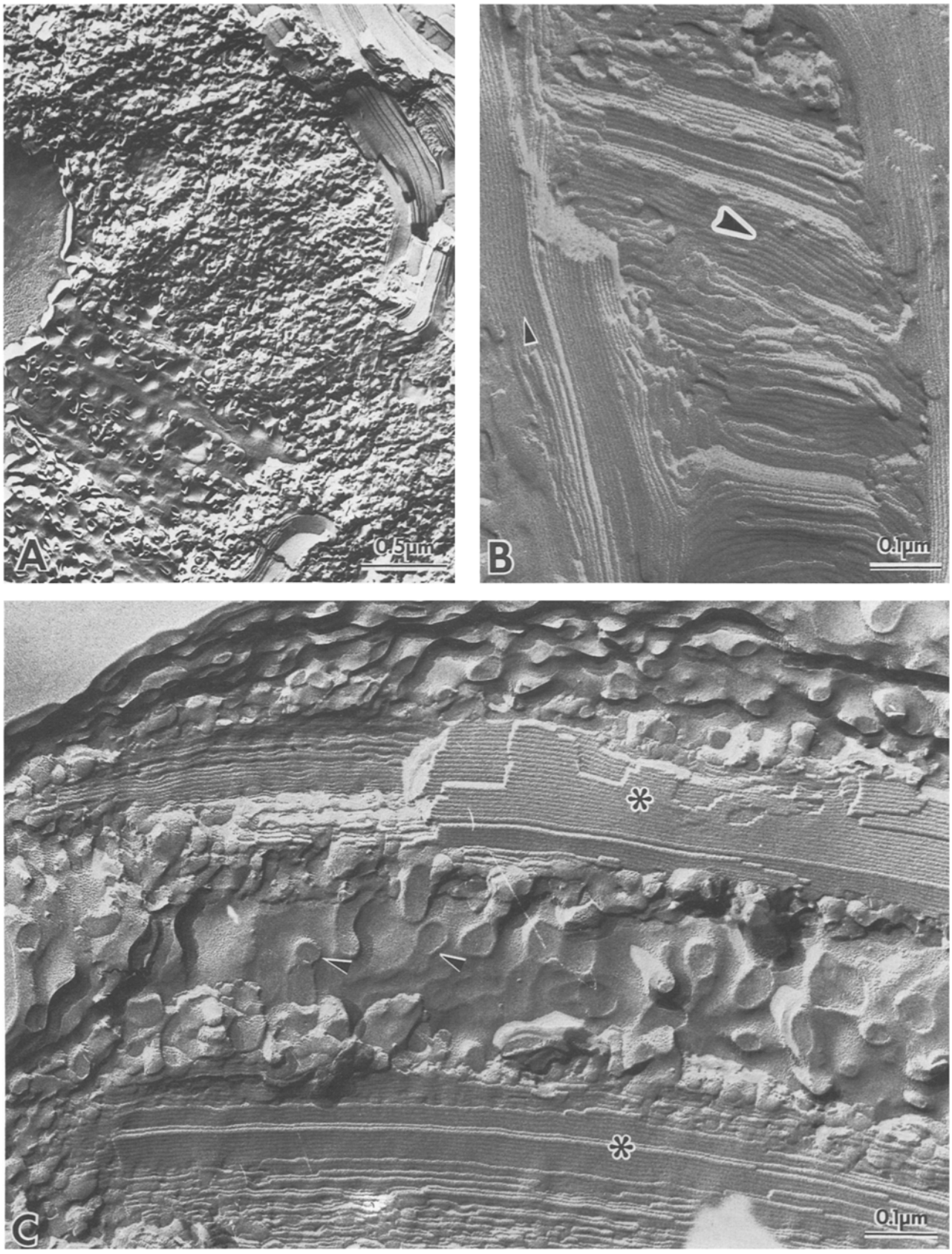

Fig. 4. Freeze-fracture images of a suspension of 1:1 molar ratio PC/CL 26 hr after the addition of calcium chloride

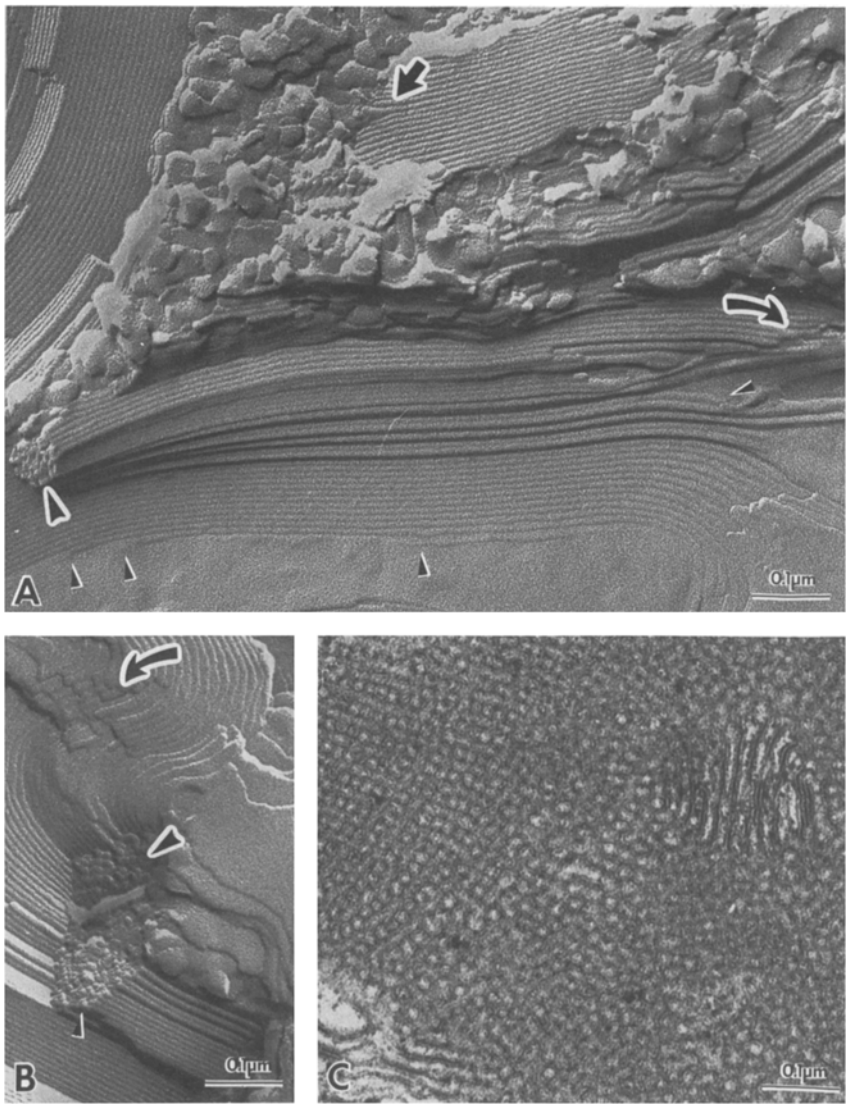

Fig. 5. Freeze-fracture (*A* and *B*) and thin-section (*C*) images of a suspension of 1:1 molar ratio PC/CL 26 hr after the addition of calcium chloride

array of rods in longitudinal fracture. However, in other areas (Fig. 5*A*, small arrowheads and curved arrow) the striations can be seen to be merging with flat, bilayer fractures. A direct continuity between a vesicle and a striation is marked by the arrow in Fig. 5*A*. At that point one of the tubules appears to rise out of the striated region, increase its diameter by a factor of two or three, and end in a round, flask-shaped structure. The appearance of this material in sections is seen in Fig. 5*C*. Closely packed bilayer tubules, with an average diameter of about 12 to 15 nm, take up most of the field. This is approximately the same diameter as the tubules observed in cross fracture in Fig. 5*B* (large arrowhead). Smaller tubules are also seen in cross section as shown in Fig. 6*B*. In this case, the tubules have diameters on the order of 10 to 12 nm. When cut in cross section (area marked by asterisks in Fig. 6*B*), the tubules consist of a dark staining central core, about 2 nm in diameter, surrounded by a clear staining ring about 3 nm in thickness and an outer dark staining ring about 2 nm in thickness. Optical diffraction of this area in Fig. 6*B*, gives an hexagonal pattern (inset). Figure 6*A* is a freeze-fracture image of the same specimen. The spacing of the striations varies from 7 to 11 mm in this image. Direct continuity between vesicles, flattened vesicles, and the striated regions can be observed (arrowheads).

Figure 7 shows freeze-fracture and thin-section images of a 1:5 PC/CL mixture after 6 hr incubation with calcium. The freeze-fracture image (Fig. 7*A*) is covered by striations of two distinct types. The area marked by the asterisk contains tubules with a diameter of about 12 nm, while the striations in the rest of the field vary from 5.5 to

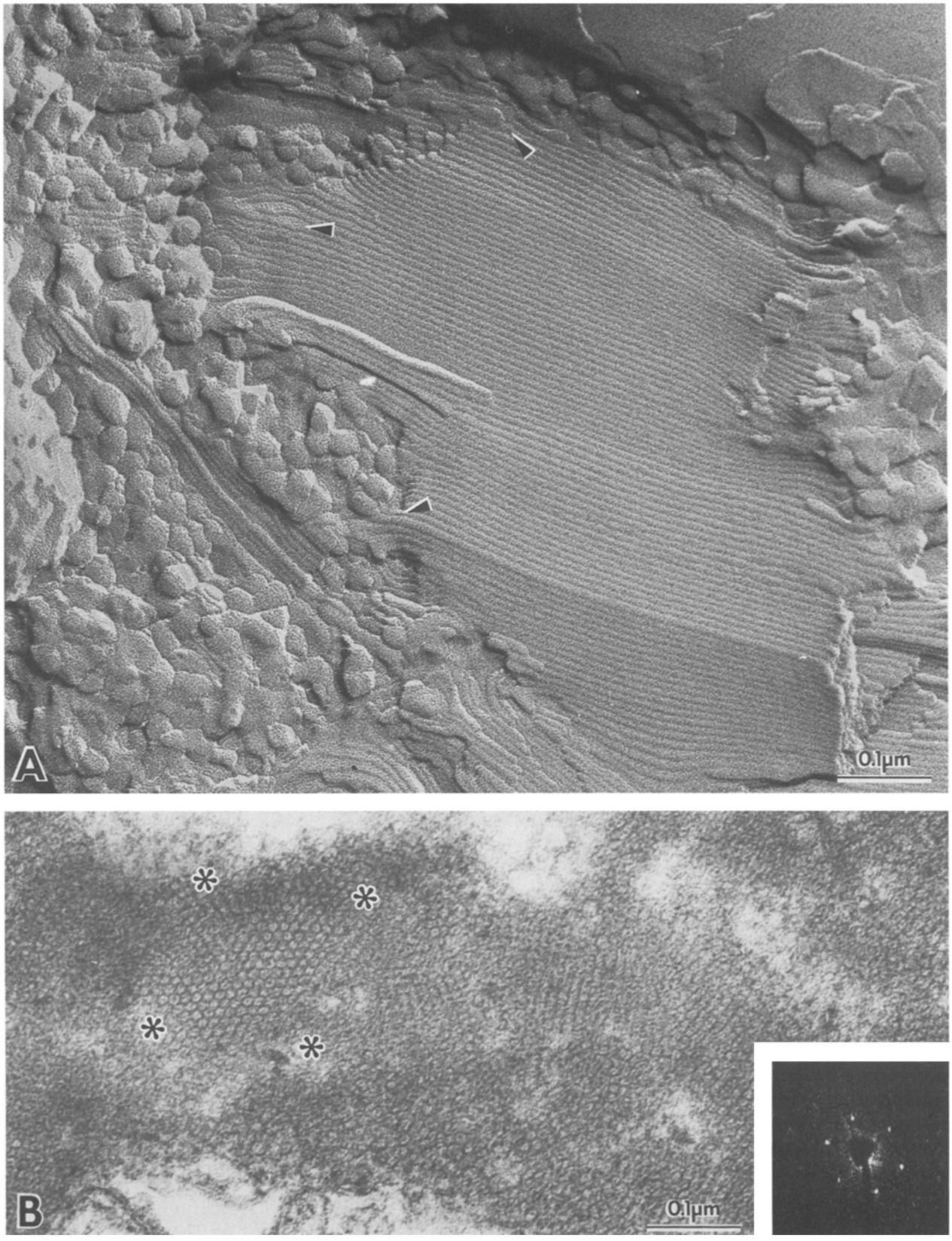

Fig. 6. Freeze-fracture (*A*) and thin-section (*B*) images of a suspension of 1:1 molar ratio PC/CL 26 hr after the addition of calcium chloride. The inset to *B* shows an hexagonal optical diffraction pattern obtained from the area marked by asterisks

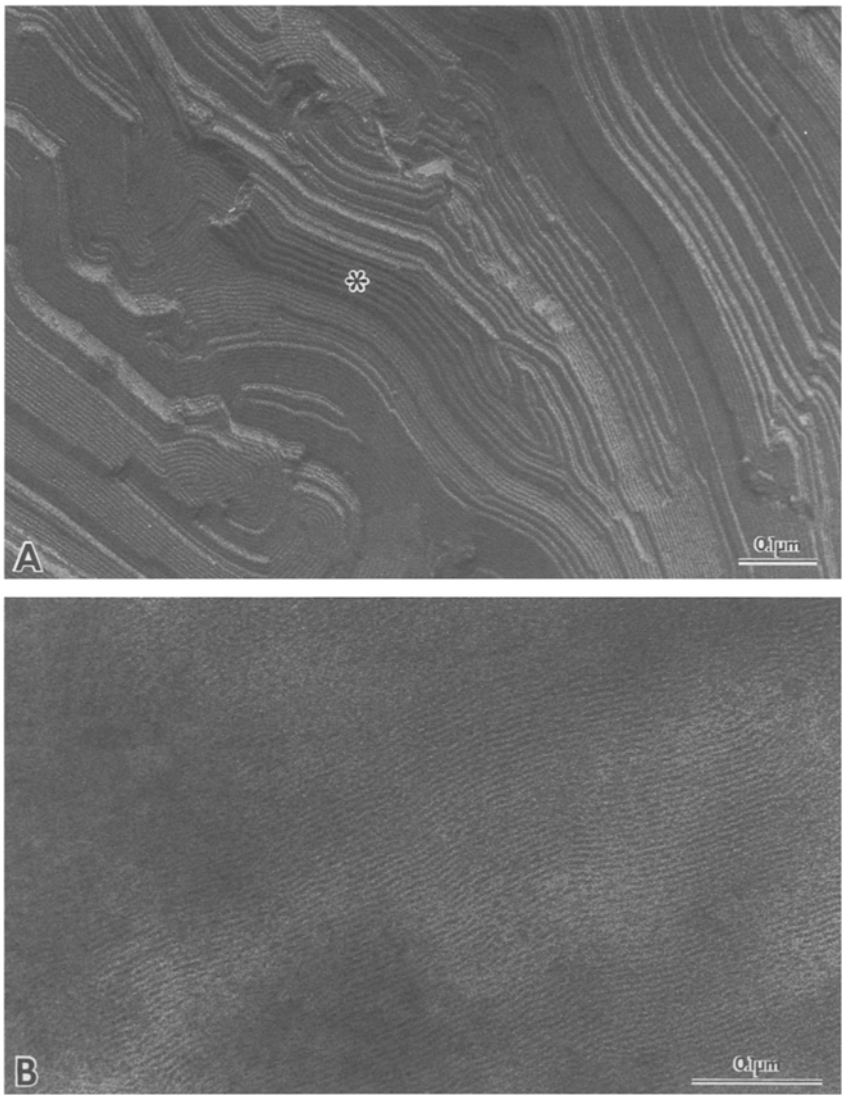

Fig. 7. Freeze-fracture (*A*) and thin-section (*B*) images of a suspension of 1:5 molar ratio PC/CL 6 hr after the addition of calcium chloride

6.0 nm and resemble in appearance previously published freeze-fracture images from the hexagonal (H_{II}) phase (Deamer, Leonard, Tardieu & Branton, 1970). In freeze-fracture replicas, the distance between striations corresponds to the distance between cyclinders (Deamer et al., 1970). In sections (Fig. 7*B*), much of the field is covered by striations having a spacing of between 5.1 and 5.5 nm. For an hexagonal phase as seen in sections, this would correspond to a separation between cylinders of 5.9 to 6.4 nm (Stoeckenius, 1962). Images of cardiolipin in the presence of calcium are shown in Fig. 8. The striations of the hexagonal phase in Fig. 8*A* have a spacing of about 5.0 to 5.5 nm and cross fractures can be seen (circle). In the thin section of Fig. 8*B*, a variety of images are obtained, depending on the orientation of the tubes relative to the plane of section. The most common image is the tubes cut in oblique section. However, in certain areas (circles) the hexagonal phase cut approximately in cross section can be seen. These areas consist of an hexagonal array of dark staining dots on a lightly staining background. The diameter of the stained dots is about 2 nm, while the center-to-center spacing of the dots is about 5.0–5.5 nm (*see* Table 1).

Mixtures of 1:1, 1:3, and 1:5 PC/CL incubated with calcium all give similar images as shown in Figs. 1–7; that is, all the intermediate stages in hexagonal phase formation, as well as the hexagonal phase itself, can be seen with these mixtures. One difference among the different preparations is the spacing of the striations in the closest packed configuration. The smallest spacing that can be observed in freeze-fracture images is about 6.5 to 7.5 nm for 1:1 PC/CL and 5.0 to 5.5 nm for car-

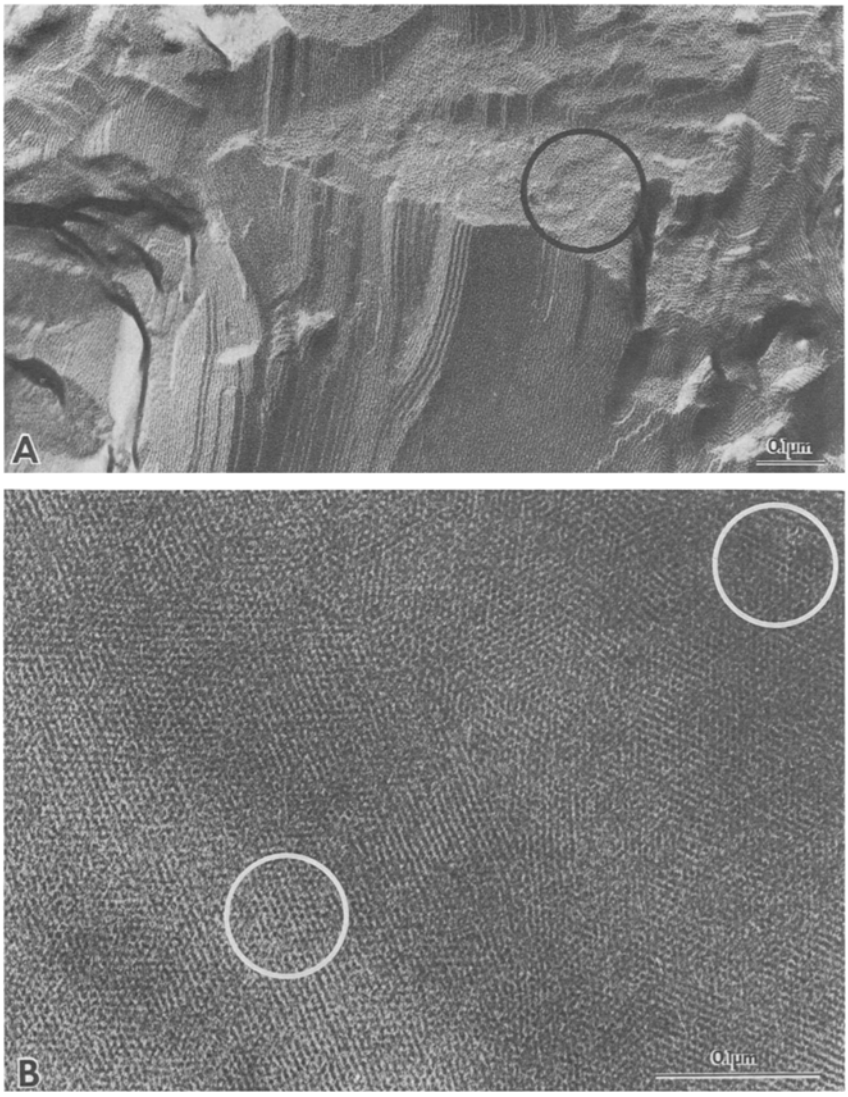

Fig. 8. Freeze-fracture (*A*) and thin-section (*B*) images of a suspension of pure cardiolipin hydrated in a 20 mM $CaCl_2$. The specimen in *A* was etched for 15 sec

Table 1. Distance between cyclinder axes in hexagonal phase (nm)

	1:1 PC/CL	1:5 PC/CL	Cardiolipin
Freeze-fracture	7.0±0.5	5.8±0.4	5.3±0.5
Thin section	–	6.2±0.4	5.3±0.4
X-ray diffraction	7.2±0.1	5.9±0.2	5.7±0.2

diolipin in calcium (*see* Table 1). At higher amounts of PC (a 3:1 PC/CL mixture) the hexagonal phase has not been observed even after 26 hr incubation in 20 mM $CaCl_2$. However, the initial stages of bilayer fusion and vesicle "pinching-off" can be observed (Fig. 9). In Fig. 9*A* one can see the lipidic particles (arrowhead) and crater-like structures (arrow) associated with the fusion of bilayers (Miller, 1980; Hui, Stewart, Boni & Yeagle, 1981; Rand et al., 1981) and the pinching-off of vesicles. Figures 9*B* and *C* show small vesicles and tubes, sometimes closely packed, in freeze-fracture and thin-section preparations.

X-ray diffraction patterns were recorded from some of the same specimens as examined by electron microscopy (Figs. 1–9). Hexagonal diffraction patterns were not detected from samples of 1:1 and 1:3 PC/CL after short (2–6 hr) incubation with $CaCl_2$ or 3:1 PC/CL after short or long (26 hr) incubation with $CaCl_2$. However, after long (26 hr) incubation in 20 mM $CaCl_2$, 1:1 and 1:5 PC/CL mixtures and pure cardiolipin all gave reflections which indexed as d, $d/\sqrt{3}$, and $d/2$. These patterns are indicative of hexagonal phases. The distances between tubes, (equal to $2d/\sqrt{3}$) are 7.2, 5.9, and 5.7 nm for 1:1 PC/CL, 1:5 PC/CL, and cardiolipin, respectively (*see* Table 1). These

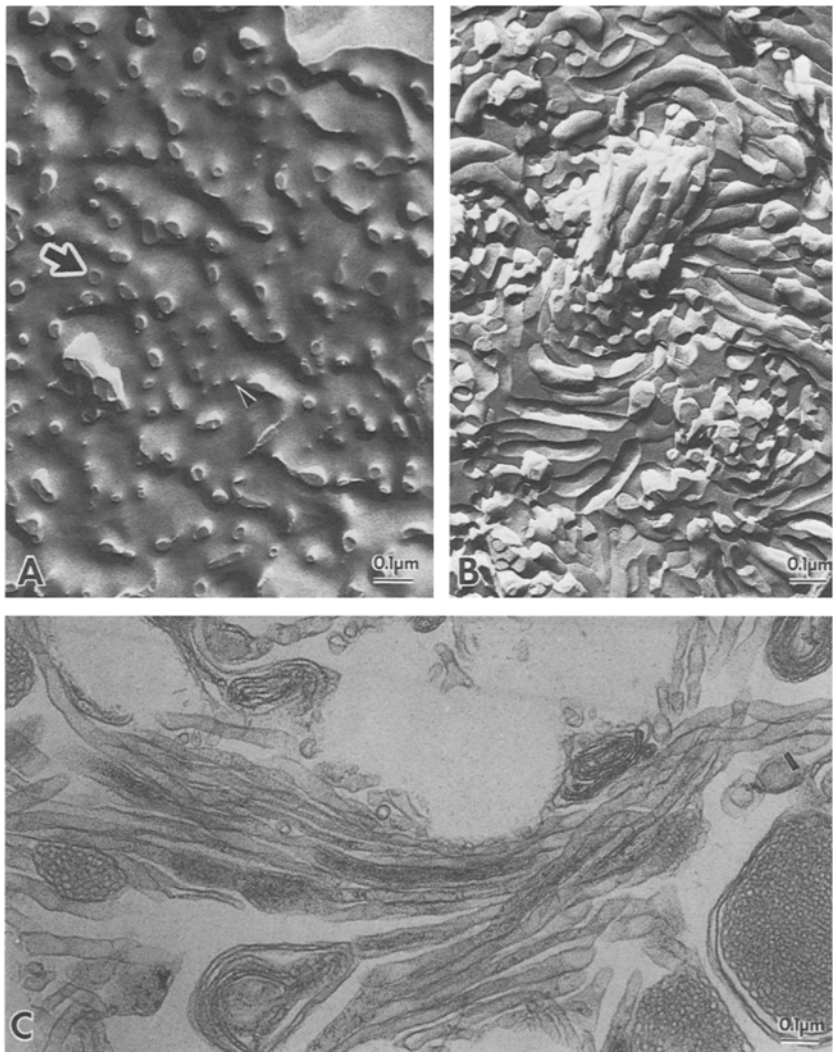

Fig. 9. Freeze-fracture (*A* and *B*) and thin-section (*C*) images of a suspension of 3:1 molar ratio PC/CL 26 hr after the addition of calcium chloride. No hexagonal (H_{II}) phase was visible in these preparations

results are very similar to the data of Rand and Sengupta (1972).

Discussion

Our results show that there are several intermediate stages in the bilayer to hexagonal phase transformation. We have attempted to summarize our data in the drawings in Fig. 10. The first stages of the transformation, depicted in Fig. 10*A*, involve outpocketing and invaginations of the outer layers of the PC/CL liposomes. Close contact and fusion between adjacent bilayers leads to a pinching-off of tubules and small, often flattened, vesicles (Fig. 10*B–D*). As noted by Rand et al. (1981), calcium probably induces a lateral segregation of lipid with the flat areas containing primarily neutral lipid and the curved bilayers containing charged lipid. These early stages can be seen in the micrographs in Figs. 1 and 2. The crater-like indentations on the fracture surface which correspond to the outpocketing and vesicle pinching-off process are seen in Fig. 4*C*. These early steps can also be observed in suspensions containing larger amounts of PC (3:1 PC/CL mole ratio) where the hexagonal phase is not formed. Figure 9*A* shows the punctate and crater-like images depicted in our drawings in Fig. 10*A* and *B*. Where the PC/CL ratio is 1.0 or less, the next stage is the formation of a tubular system (Fig. 10*E* and 10*E'*). It appears that the tubular system can arise either from small vesicles or from larger flattened vesicles. Direct continuities between tubular system and small vesicles can be seen in Figs. 3*D*, 5*A*, and 6*A*. Continuities between flattened vesicles and the tubular system are shown in Fig. 3*B* and *D* and Fig. 5*A–C*. In some areas, such as in Figs. 3*D* (arrow) and 5*A* (arrowheads), the flattened vesicular system has a striated

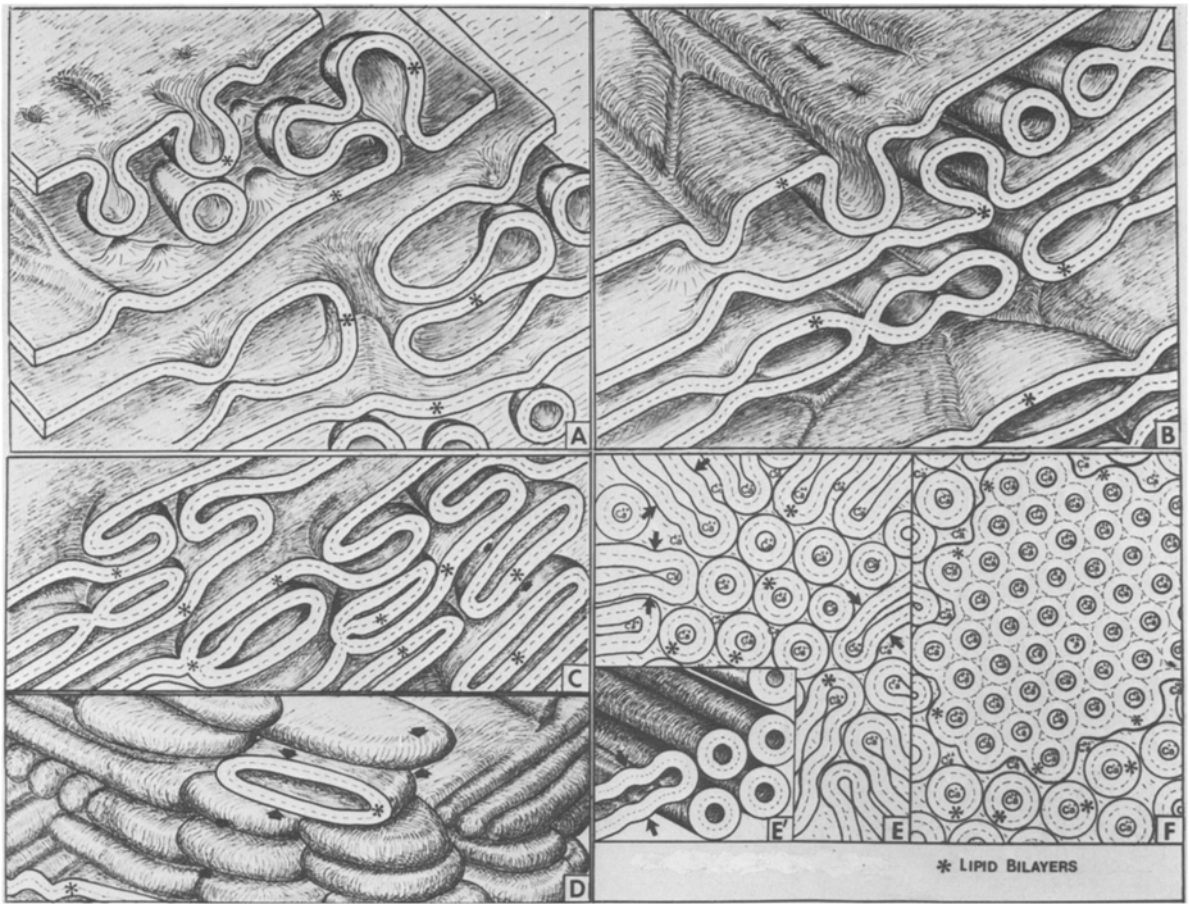

Fig. 10. Three-dimensional drawings of our interpretation of the intermediate stages in the lamellar to hexagonal (H_{II}) phase transition. Lipid bilayers are denoted by asterisks, and dotted lines are placed in hydrophobic regions of the bilayers and hexagonal phases. The bilayer-enclosed tubes drawn in cross section in the center of *E* make up the "complex Hexagonal" phase, while the tubes of the hexagonal (H_{II}) phase are shown in cross section in *F* (*See* text for details)

appearance as it merges with the tubular system. Our interpretation of this phenomenon is shown in Fig. 10*E'*. It is often difficult to tell precisely where the flattened vesicular system ends and where the tubular arrangement begins, unless cross fractures are present. The cross fractures denoted by large arrowheads in Fig. 5*A* and *B* are distinctively tubular in nature, while the fractures denoted by the curved arrows in Fig. 5*A* and *B* appear to be from flattened, striated vesicles.

We have found two distinct types of tubular systems. The first type has a tubule diameter of between 10 and 15 nm. In sections, the largest of these structures appears to be composed of bilayer enclosed cylinders (Fig. 5*C*, depicted in Fig. 10*E* and *E'*). These large tubules (14–15 nm) have an irregular packing. However, somewhat smaller bore tubules (10–11 nm in diameter) are often packed in an hexagonal array (Fig. 6*B*). We believe that the smaller tubules arise from the large tubules by a further dehydration of the fluid space by calcium. For the smaller bore tubules, the fluid space in the center of the tubules is extremely small and only a 2-nm dot of stain can be seen in the center of each tube. It is important to realize that each tube is surrounded by a hydrophilic stain-filled matrix. We interpret this class of tubule to be closely packed cyclinders formed from bilayers. This type of bilayer tubular arrangement was classified as "complex hexagonal" by Luzzati and Husson (1962). We believe this is the first time the complex hexagonal phase has been analyzed by electron microscopy. Large 14-nm tubes were also described by Van Venetie und Verkleij (1981) in their freeze-fracture analysis of the transition from bilayer to hexagonal phase. They did not have the benefit of thin-section images and classified these large tubules as hexagonal (H_{II}) phase. However, hexagonal (H_{II}) phase tubules can not be surrounded by a hydrophilic matrix (Luzzati & Husson, 1962) as seen in Fig. 6*C*.

The second class of tubules that we observe

has a spacing between cylinders of between 7.5 and 5.0 nm, depending on the PC/CL ratio. The dimensions obtained by X-ray diffraction, freeze-fracture, and thin sectioning are in good agreement (*see* Table 1). It has previously been shown by Rand and Sengupta (1972) that the dimensions of these phases depend strongly on the PC/CL ratios and are practically independent of the concentration of the precipitating solution of $CaCl_2$. Freeze-fracture and thin-section views of this phase are shown in Figs. 7 and 8 and depicted in Fig. 10*F*. The dimensions and appearance of these tubules are characteristic of hexagonal (H_{II}) phases (Deamer et al., 1970; Rand & Sengupta, 1972). Note in particular that cross sections of this phase (as circled in Fig. 8*B*) show hexagonal arrays of dots of stain surrounded by a pale hydrophobic matrix. In addition, the cross fractures of the hexagonal (H_{II}) phase (Fig. 8*A*, circle) are quite different in appearance and dimensions from the cross fractures we have observed from the larger tubes of the complex hexagonal phase (Fig. 5*A* and *B*, large arrowheads). In Fig. 7, most of the field is covered by the fine striations characteristic of the hexagonal (H_{II}) phase. However, a small region (marked by an asterisk) contains larger bore tubules which may be complex hexagonal phase. The hexagonal (H_{II}) phase is the predominant phase seen after long (26 hr) incubation time with $CaCl_2$. The complex hexagonal, which is usually seen with shorter incubation times with $CaCl_2$, appears to be an intermediate phase in the bilayer to hexagonal transition for the PC/CL system. Luzzati and Husson (1962) found that the complex hexagonal phase was an intermediate phase in the lamellar to hexagonal transition for certain soaps, but as far as we know this is the first time the complex hexagonal phase has been described for phospholipids.

The mechanism for conversion of the complex hexagonal to the hexagonal phase is not fully understood at present. A further dehydration by calcium must be part of the process. There are at least three possibilities for the geometry of the conversion. First, the hexagonal phase may form by a pinching-off process in a direction perpendicular to the axes of the complex hexagonal tubules. Secondly, the hexagonal phase cylinders might flow lengthwise from the complex hexagonal tubules. This would be consistent with the expected flow anisotropy of tubular liquid crystalline phases. A third possibility is that the calcium might dehydrate and convert the complex hexagonal tubules to the hexagonal phase without the bulk flow of lipid.

Lipidic particles, as described in several previous studies, can be seen in the early stages of the bilayer to hexagonal transformation. As noted by Miller (1980), they appear to be involved in the initial fusion processes between adjacent bilayers in the PC/CL liposomes. An important finding of our work is that the intermediate stages in the bilayer to hexagonal transformation all involve some type of bilayer enclosed structure.

VLB would like to express his deep thanks to Dr. J.D. Robertson (Duke University) and to Diane Breliauskas (National Academy of Science, USA) for their hospitality and support during his stay in the United States and to Dr. Robertson for many stimulating discussions and for use of his research facilities during the course of this research. This research was performed while Dr. Borovjagin was in the United States as part of the joint exchange between the National Academy of Sciences of the U.S. and the Soviet Academy of Science. This work was also funded by National Institutes of Health grants GM/AM 28224 (to J.D. Robertson) and GM 27278 (to TJM). We thank Mrs. Pat Thompson for a fine job of typing this manuscript.

References

Borovjagin, V.L., Vasilenko, I.A. 1981. ^{31}P-NMR and freeze-fracture electron microscopy studies of model lipid membranes in relation to lipidic intramembrane particles. *Anat. Rec.* **19313**:32*A*

Buchheim, W., Drenckhahn, D., Lullmann-Rauch, R. 1979. Freeze-fracture studies of cytoplasmic inclusions occurring in experimental lipidosis as induced by amphiphilic cationic drugs. *Biochim. Biophys. Acta* **575**:71–80

Burnell, E., Van Alphen, L., Verjleij, A., DeKruijff, B. 1980. ^{31}P nuclear magnetic resonance and freeze-fracture electron microscopy studies on *Escherichia coli*. I. Cytoplasmic membrane and total phospholipids. *Biochim. Biophys. Acta* **597**:492–501

Corless, J.M., Costello, M.J. 1981. Paracrystalline inclusions associated with the disk membranes of frog retinal rod outer segments. *Exp. Eye Res.* **32**:217–228

Costello, M.J. 1980. Ultra-rapid freezing of thin biological samples. *Scanning Elec. Microsc.* **2**:361–370

Costello, M.J., Corless, J.M. 1978. The direct measurement of temperature changes within freeze-fracture specimens during rapid quenching in liquid coolants. *J. Microsc.* **112**:17–37

Cullis, P.R., Hope, M.J. 1978. Effects of fusogenic agent on membrane structure of erythrocyte ghosts and the mechanism of membrane fusion. *Nature (London)* **271**:672–674

Cullis, P.R., DeKruijff, B. 1979. Lipid polymorphism and the functional roles of lipids in biological membranes. *Biochim. Biophys. Acta* **559**:399–420

Cullis, P.R., DeKruijff, B., Hope, M.J., Nayar, R., Rietweld, A., Verkleij, A.J. 1980. Structural properties of phospholipids in the rat liver inner mitochondrial membrane. A ^{31}P-NMR study. *Biochim. Biophys. Acta* **600**:625–635

Deamer, D.W., Leonard, R., Tardieu, A., Branton, D. 1970. Lamellar and hexagonal lipid phases visualized by freeze-etching. *Biochim. Biophys. Acta* **219**:47–69

DeGrip, W.J., Drenthe, E.H.S., Van Echteld, C.J.A., DeKruijff, B., Verkleij, A.J. 1979. A possible role of rhodopsin in maintaining bilayer structure in the photoreceptor membrane. *Biochim. Biophys. Acta* **558**:330–337

Gulik-Krzywicki, T., Rivas, E., Luzzati, V. 1967. Structure et polymorphisme des Lipides: Etude par diffraction des rayons X du systeme forme de lipides de mitochondries de Coeur de boeuf et d'eau. *J. Mol. Biol.* **27**:303–322

Hui, S.W., Stewart, T.P., Boni, L.T., Yeagle, P.L. 1981. Membrane fusion through point defects in bilayers. *Science* **212**:921–923

Hui, S.W., Stewart, R.P., Yeagle, P.L., Albert, A.D. 1981. Bilayer to non-bilayer transition in mixtures of phosphatidylethanolamine and phosphatidylcholine: Implications for membrane properties. *Arch. Biochem. Biophys.* **207**:227–240

Junger, E., Reinauer, H. 1969. Liquid crystalline phases of hydrated phosphatidylethanolamine. *Biochim. Biophys. Acta* **183**:304–308

Kalina, M., Pease, D.C. 1977. The preservation of ultrastructure in saturated phosphatidylcholines by tannic acid in model systems and type II pneumocytes. *J. Cell Biol.* **74**:726–741

Luzzati, V., Husson, F. 1962. The structure of the liquid-crystalline phases of lipid-water systems. *J. Cell. Biol.* **12**:207–218

McIntosh, T.J., Simon, S.A., MacDonald, R.C. 1980. The organization of *n*-alkanes in lipid bilayers. *Biochim. Biophys. Acta* **597**:445–463

Miller, R.G. 1980. Do "lipidic particles" represent intermembrane attachment sites? *Nature (London)* **287**:166–167

Rand, R.P., Reese, T.S., Miller, R.G. 1981. Phospholipid bilayer deformations associated with interbilayer contact and fusion. *Nature (London)* **293**:237–238

Rand, R.P., Sengupta, S. 1972. Cardiolipid forms hexagonal structures with divalent cations. *Biochim. Biophys. Acta* **255**:484–492

Stoeckenius, W. 1962. Some electron microscopical observations on liquid-crystalline phases in lipid water systems. *J. Cell Biol.* **12**:221–229

Tardieu, A., Luzzati, V., Reman, F.C. 1973. Structure and polymorphism of the hydrocarbon chains of lipids: A study of lecithin-water phases. *J. Mol. Biol.* **75**:711–733

Van Venetie, R., Verkleij, A.J. 1981. Analysis of the hexagonal H_{II} phase and its relations to lipidic particles and the lamellar phase. A freeze-fracture study. *Biochim. Biophys. Acta* **645**:262–269

Verkleij, A.J., Mombers, C., Gerritsen, W.J., Leunissen-Bijvelt, L., Cullis, P.R. 1979. Fusion of phospholipid vesicles in association with the appearance of lipidic particles as visualized by freeze fracturing. *Biochim. Biophys. Acta* **555**:358–361

Verkleij, A.J., Van Echteld, C.J.A., Gerritsen, W.J., Cullis, P.R., DeKruijff, B. 1980. The lipidic particle as an intermediate structure in membrane fusion processes and bilayer to hexagonal H_{II} transitions. *Biochim. Biophys. Acta* **600**:620–624

Received 26 January 1982; revised 4 May 1982